# Influence of Nanoscale Phase Separation on the Charge Generation Dynamics and Photovoltaic Performance of Conjugated Polymer Blends: Balancing Charge Generation and Separation

**ARTICLE** *in* THE JOURNAL OF PHYSICAL CHEMISTRY C · DECEMBER 2007

Impact Factor: 4.77 · DOI: 10.1021/jp075904m



**5 AUTHORS**, INCLUDING:

Christopher R. McNeill
Monash University (Australia)
**112** PUBLICATIONS **3,803** CITATIONS
SEE PROFILE

Sebastian Westenhoff
University of Gothenburg
**39** PUBLICATIONS **1,512** CITATIONS
SEE PROFILE

# Influence of Nanoscale Phase Separation on the Charge Generation Dynamics and Photovoltaic Performance of Conjugated Polymer Blends: Balancing Charge Generation and Separation

**Christopher R. McNeill,* Sebastian Westenhoff, Chris Groves, Richard H. Friend, and Neil C. Greenham**

*Cavendish Laboratory, Department of Physics, University of Cambridge, J J Thomson Ave, Cambridge CB3 0HE, United Kingdom*

*Received: July 26, 2007; In Final Form: October 10, 2007*

Through controlled annealing of intimately mixed blends of the polyfluorene copolymers poly(9,9′-dioctylfluorene-*co*-bis(*N*,*N*′-(4,butylphenyl))bis(*N*,*N*′-phenyl-1,4-phenylene)diamine) (PFB) and poly(9,9′-dioctylfluorene-*co*-benzothiadiazole) (F8BT) we observe the change in charge generation dynamics and photovoltaic performance as the length of nanoscale phase separation is varied from 5 nm or less to greater than 40 nm. We find that device efficiency is optimized for a phase separation of ∼20 nm, significantly larger than the exciton diffusion length of ∼5−10 nm. Femtosecond time-resolved transient absorption measurements confirm that the charge generation time is longer and charge generation efficiency is lower in films with a more evolved morphology. Photoluminescence quantum efficiency is also observed to monotonically increase with annealing temperature consistent with a decrease in exciton dissociation resulting from a coarsening of phases. Using a Monte Carlo model of exciton diffusion and dissociation in computer-simulated structures, we infer that the domains have purity of >95% and find good agreement between the observed photoluminescence quenching and measured domain sizes. Charge transport studies of single-carrier devices show that charge transport through the blend does not significantly improve as device performance improves, and photocurrent is observed to scale linearly with light intensity independent of blend morphology and device geometry. We conclude that the recombination of geminate charge pairs is limiting device performance, with the optimum phase separation of 20 nm balancing the efficiency of charge generation and charge separation.

## Introduction

Organic solar cells are a promising route to low-cost photovoltaic technology.[1] To date the most efficient devices are achieved using blends of a conjugated polymer and methanofullerene, with efficiencies of order 6% under solar conditions.[2,3] Polymer/polymer blends,[4] which were demonstrated at the same time as polymer/fullerene blends[5] but currently show lower efficiencies (∼2%[6]), are still of interest due to their higher open-circuit voltage and the potential to create ordered nanostructures through block copolymers.[7,8] While ideal photovoltaic structures have been proposed[1] with interdigitated, pure phases interspaced by a distance equal to or less than the exciton diffusion length (typically between 5 and 10 nm[9−11]), there are few experimental reports on the influence of nanoscale phase separation on photovoltaic performance.

Blends of the polyfluorene copolymers PFB and F8BT have provided a useful prototype system for the study of photophysics and charge generation dynamics in all-polymer solar cells.[12−17] Charge generation proceeds via the dissociation of excitons at PFB/F8BT interfaces to form coulombically bound geminate electron−hole pairs. These geminate pairs may either relax to an exciplex state, with a certain proportion decaying radiatively with characteristic red-shifted emission, or may undergo charge separation.[16,17] For efficient device operation, separation of geminate electron−hole pairs into free charges must be favored over geminate recombination. Despite the attention received by PFB:F8BT blends, external quantum efficiencies (EQE) have remained low, typically less than 4% under short-circuit conditions. These low efficiencies suggest that a fundamental property of this material combination, such as the difficulty dissociating geminate electron−hole pairs, limits the overall efficiency.

Studies of the operation of PFB:F8BT devices have largely focused around the influence of blend morphology on device performance.[12−14,18−20] Blends prepared from chloroform that have an intimate mixing of the two polymers on the scale of less than 10 nm have been found to outperform devices prepared from xylene that exhibit coarser micrometer-sized domains.[18] These differences were initially explained in terms of the coarser, mesoscale morphology of the xylene blend with charge separation and collection efficient only at micrometer-sized domain boundaries.[13] However, subsequent near-field photocurrent[19] and electrostatic force microscopy[20] studies have shown directly that the majority of photocurrent originates from within the micrometer-sized domains in xylene-prepared blends. These results, along with the observation by X-ray microscopy that the mesoscale domains still contain a significant degree of intermixing,[21,22] have demonstrated that device performance is determined by the degree of phase separation on the nanoscale.

In order to bridge these studies of morphology[12−14,18−20] and charge generation dynamics,[16,17] we have investigated the

* To whom correspondence should be addressed. Tel: +44 (0)1223 337285. Fax: +44 (0)1223 764515. E-mail: crm51@cam.ac.uk.

10.1021/jp075904m CCC: $40.75 
Published on Web 12/04/2007 PAGE EST: 7.5

influence of nanoscale morphology on charge generation and collection through controlled annealing of intimately mixed PFB:F8BT blends. Steady-state photoluminescence measurements and femtosecond transient absorption studies are used to probe the efficiency and kinetics of charge generation, while device efficiency, single-carrier transport, and light-intensity dependent measurements are used to separate the processes of charge transport and geminate pair separation.

## Experimental Methods

PFB:F8BT blends were prepared from chloroform solutions with a weight ratio of 1:1 and deposited by spin-coating at a concentration of 8 mg/mL in chloroform to form 80 nm thick films. Molecular weights of $M_p = 135$ kg/mol and $M_p = 150$ kg/mol for PFB and F8BT, respectively, were used. Films were either spin-coated onto poly(3,4-ethylenedioxythiophene):polystyrene sulfonic acid (PEDOT:PSS) coated indium tin oxide/glass substrates for device fabrication or glass/quartz substrates for optical characterization. Annealing was performed by placing substrates or devices on a hotplate in a nitrogen glove box for 10 min followed by rapid cooling to room temperature. For the case of devices, annealing was performed on completed devices (with aluminum electrodes evaporated at a base pressure of less than $10^{-6}$ mbar) before encapsulation and device testing. Single-carrier hole-only devices were fabricated identically except with the use of a gold electrode in place of aluminum.

Atomic force microscopy (AFM) was performed with a Digital Instruments Nanoscope IIIa in noncontact mode. AFM was performed on films annealed in completed device geometries with the aluminum electrode subsequently removed using adhesive tape to reveal the underlying polymer blend morphology. AFM measurements of annealed films on glass/quartz substrates revealed similar systematic changes in morphology with annealing (see Supporting Information for more detail).

Device external quantum efficiency (EQE) was measured as a function of wavelength at intensities of ~1 mW/cm$^2$, with short-circuit current recorded using a Keithley 237 source measure unit (SMU). Monochromatic light was provided by a tungsten filament dispersed through a monochromator with a spot size smaller than the device active area (4.5 mm$^2$). Incident light intensity was continuously monitored during measurement and calibrated by a Hamamatsu S8746-01 photodiode. Current−voltage measurements were also performed using a Keithley 237 SMU, either under AM1.5 irradiation (Oriel 81160-1000 solar simulator) or in the dark on hole-only devices. For intensity dependence measurements, light was provided by a 470 nm high-intensity LED with intensity moderated by neutral density filters.

Photoluminescence (PL) spectra and efficiencies were measured at room temperature in a nitrogen-purged integrating sphere with excitation from an argon ion laser at 488 nm and detection with an Oriel Instraspec IV spectrometer. PL efficiencies were calculated as described by de Mello et al.[23]

Femtosecond transient absorption measurements were performed utilizing two optical paramagnetic amplifiers (OPAs) seeded by the 800 nm output (pulse duration <80 fs) of a commercially available oscillator/amplifier system (Tsunami and Spitfire Pro, Spectra Physics). The pump pulses were generated using a TOPAS (Light Conversion) and were centered at 490 nm with a full width half-maximum of 10 nm. The broadband probe light spanning from 530 to 750 nm was generated with a home-built noncollinear OPA following the setup outlined in ref 24. Differential transient transmission ($\Delta T/T$) spectra were measured by spectrally resolving probe and reference pulses in a spectrograph and recording the light intensity with two diode arrays. The 256 pixel array (S3901256Q, Hamamatsu) was read out using a commercially available circuit at 2 MHz (C7844, Hamamatsu) and digitized for each laser pulse using a PXI-6122 card (National Instruments). The transmission with excitation light on and off ($T_{on}$ and $T_{off}$) was calculated using a stand alone computer with a real-time operating system (PXI-8175 and Labview real-time) and recorded as a function of optical delay between pump and probe. The data were corrected for chirp of the probe and the offset at negative time was subtracted. The time resolution was ~120 fs as judged from the rise time of the signal. F8BT was selectively excited at 490 nm in all experiments.

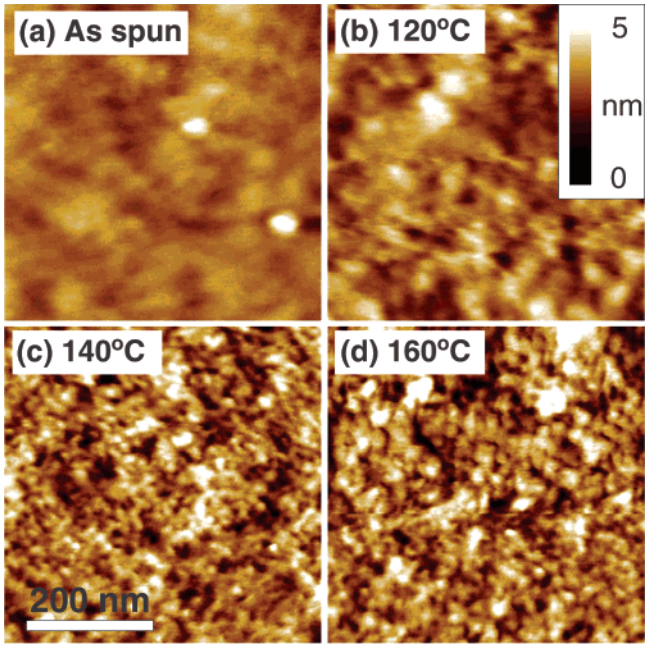


**Figure 1.** Evolution of the nanoscale morphology of PFB:F8BT blends spin-coated from chloroform with subsequent annealing as imaged by AFM: (a) as-spun film; (b) film annealed at 120 °C; (c) film annealed at 140 °C; (d) film annealed at 160 °C. The images display the surface topography (height) and share the same scale bars.

## Results and Discussion

Figure 1 shows AFM images of typical annealed blends used in this study. Figure 1 shows that varying the anneal temperature from 120 to 160 °C allows for control of the morphology of the blend. In particular, for the as-spun and 120 °C annealed films the phase separation is on the length scale of 10 nm or less and is not easily resolved. For the 140 and 160 °C annelaed films a distinct phase separation is observed, with domain sizes of 18 ± 4 and 35 ± 8 nm, respectively, measured from cross-sectional profiles. The evolution of morphology over this temperature range is in agreement a glass transition temperature of ~140 °C for F8BT and PFB.[25,26] Annealing was performed on other samples up to 220 °C producing an even greater degree of phase separation. Variation of the morphology in this way is preferable to varying morphology by varying the blend ratio as a uniform blend composition and hence optical absorption (see Supporting Information) is maintained over all devices.

Figure 2 presents the influence of annealing on device performance. Figure 2 shows that device performance improves with annealing, with device EQE increasing from 3.5% in as-spun blends to 6% for an anneal temperature of 140 °C. Annealing also has a mild influence on device open-circuit voltage and fill factor, with fill factor increasing from 0.27 to

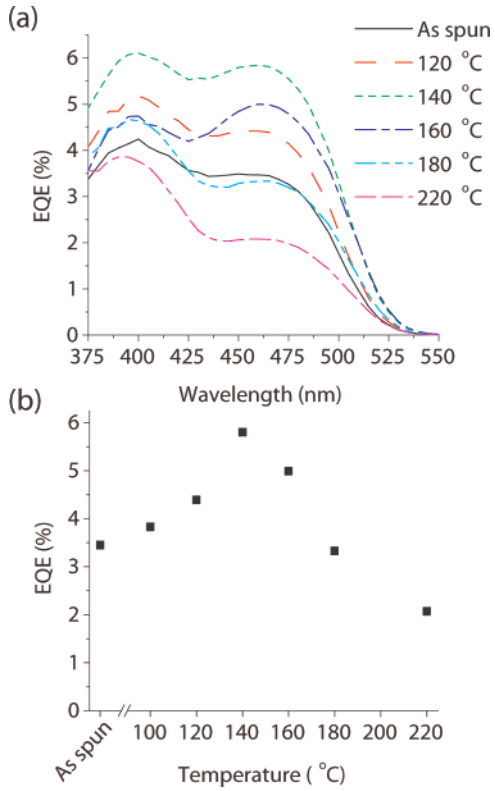


**Figure 2.** Influence of device annealing on the performance of PFB:F8BT blend devices: (a) spectral response of device external quantum efficiency; (b) external quantum efficiency at 465 nm.

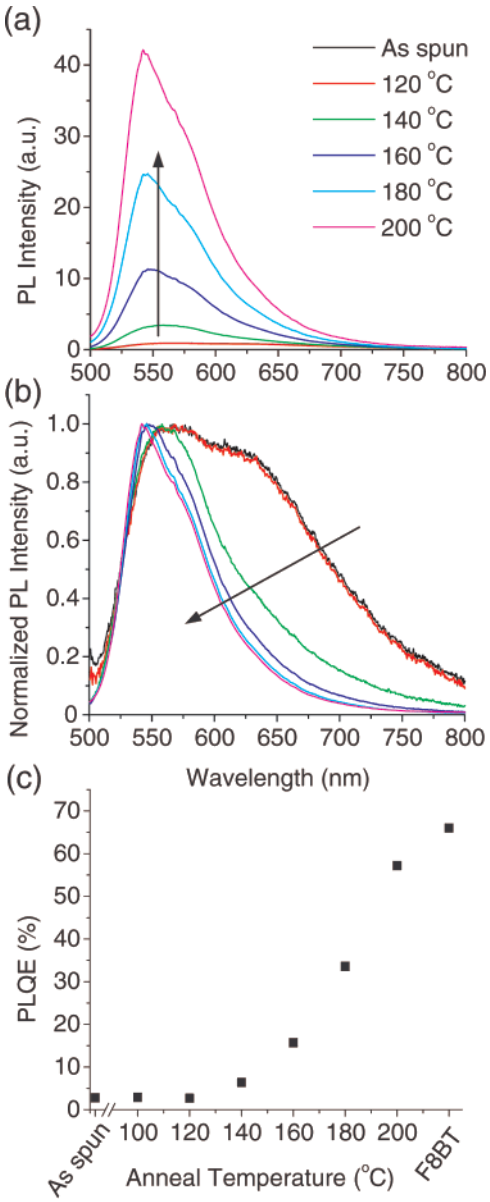


**Figure 3.** Influence of anneal temperature on the photoluminescence of PFB:F8BT blend films: (a) photoluminescence spectra; (b) normalized photoluminescence spectra; (c) photoluminescence quantum efficiency. The F8BT quantum efficiency is for an annealed film. All measurements were performed in a nitrogen-purged integrating sphere with excitation at 488 nm.

0.38 and open circuit voltage increasing from 1.27 to 1.38 V with annealing (see Supporting Information). As shown in Figure 3, alongside the observed increase in device efficiency, the PL yield also increases with annealing temperature as the morphology of the blend evolves into a more phase-separated state. Above an anneal temperature of 140 °C, however, device performance deteriorates but still exceeds that of the as-spun device up to an anneal temperature of ∼180 °C. Remarkably, for an anneal temperature of 160 °C where device performance still exceeds that of the as-spun device, the PL yield of the film is more than 1 order of magnitude higher than that of the as-spun film (Figure 3a). Integrating sphere measurements of photoluminescence quantum efficiency, Figure 3c, yield a PLQE for as-spun blends of 2.8%, corresponding to a PL quenching of 95% (relative to a pristine F8BT film with PLQE of 55%). For an anneal temperature of 160 °C, PLQE increases to ∼15.7% (a PL quenching of ∼70%) indicating that despite nearly a third of photoexcited excitons now recombining radiatively before they reach a heterojunction, device performance is still improved relative to the as-spun film with 95% exciton dissociation yield. Similarly, for 180 °C annealed films, device efficiency is only slightly lower than that of the as-spun film, despite photoluminescence quenching decreasing to ∼50% (relative now to an annealed F8BT film with a higher PLQE of 66%[25]). That device performance is improved despite a marked reduction in exciton dissociation yield suggests that there is an intrinsic difficulty in either the separation of geminate electron−hole pairs or their subsequent collection in intimately mixed PFB:F8BT blends. Examining the shape of the normalized PL spectra of Figure 3b shows that the as-spun and 120 °C annealed films show significant exciplex emission, further suggesting a preference for geminate recombination over charge separation in intimately mixed blends. The PL spectrum of the 160 °C annealed film in contrast resembles that of the F8BT singlet exciton emission indicating that exciplex emission is suppressed. A similar anticorrelation between exciplex emission and device performance has also been recently reported by Yin et al., who studied poly(phenylenevinylene) (PPV) based blends.[27]

Further insight into the dynamics of exciton diffusion and charge generation in these blends are provided by the femtosecond transient absorption measurements of Figure 4. Figure 4a presents time-resolved transient absorption spectra of a film annealed at 100 °C with morphology and device performance similar to those of an as-spun film. Two major features can be observed: a positive spectral feature in the range 530−630 nm at early time replaced by a negative $\Delta T/T$ signal after a few picoseconds. In agreement with earlier work, we assign the positive signal to stimulated emission of excitons in F8BT and the negative signal to photoinduced absorption by charges on PFB and F8BT.[28,29] Panel b of Figure 4 presents the transient absorption spectra for a sample annealed at 180 °C. This film has a well-evolved morphology, and the signal in this wave-

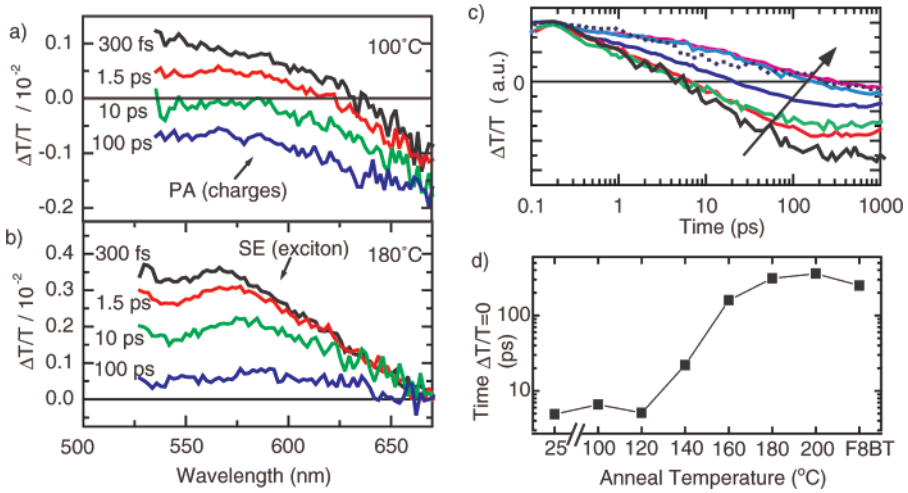


**Figure 4.** Femtosecond transient absorption measurements of annealed PFB:F8BT blends. Panels a and b show differential transmission spectra at delay times as indicated in the figure for two samples annealed at 100 and 180 °C, respectively. The spectra were integrated over a time window of less than ±20% of the time indicated in the panel. Panel c shows the same data, spectrally integrated over a wavelength region from 530 to 600 nm as a function of time, with increasing annealing temperature: 25 (as spun), 100, 120, 140, 160, and 180 °C (the kinetics at 200 °C were very similar to 180 °C and are not shown). The kinetics of a spin-cast film of F8BT only are shown as a dotted line. Panel d plots the time at which integrated $\Delta T/T$ crosses zero as a function of annealing temperature. The excitation fluence was $1 \times 10^{-14}$ photons/cm$^2$ for all measurements.

length range clearly consists only of stimulated emission. This spectrum is red-shifted by about 50 nm compared to the 100 °C annealed film consistent with the reorganization of F8BT chains with annealing.[25] We note that this red-shift, however, is much larger than the spectral shift observed for the PL and could be due to a large shift of the excitonic excited-state absorption. Importantly, broad photoinduced absorption due to charges is not observed and we conclude that charge separation does not occur within the first 100 ps. Spectrally integrated (530−600 nm) kinetics of a number of samples annealed at different temperatures are plotted in panel c. It is shown that the time at which photoinduced (charge) absorption dominates the stimulated emission signal of the excitons strongly depends on annealing temperature and hence the length scale of phase separation. This is summarized in panel d, where the time at which integrated $\Delta T/T$ crosses zero is plotted against anneal temperature. For samples annealed at $T = 120$ °C or less, annealing has very little effect on the dynamics and the zero-crossing time is almost constant at ca. 5 ps. The crossing time dramatically increases for annealing at 140 °C (22 ps) and 160 °C (160 ps), whereas at 180 and 200 °C it again levels out (at a value of ∼340 ps). As all kinetics in panel c have been normalized to the stimulated emission signal at 150 fs, the charge generation efficiency can be judged directly from the magnitude of the negative signal at late times. Gauging the charge generation efficiency in this way reveals that the efficiency of charge generation systematically decreases with increasing annealing temperature. For comparison, the transient absorption kinetics of a pristine F8BT film have been recorded and are also plotted in Figure 4c. While the pristine F8BT film possesses no heterojunctions for exciton dissociation, the kinetics of this film still changes sign after 250 ps. The presence of a photoinduced absorption signal in pristine F8BT films has been observed previously and has been assigned to charges generated by highly efficient exciton−exciton annihilation.[28] The occurrence of exciton−exciton annihilation means that for zero-crossing times larger than 250 ps this process may be the dominant mechanism for charge generation within the F8BT phases instead of charge generation at the heterojunction. Therefore, for the 180 and 200 °C annealed films the charge generation times as determined by femtosecond time-resolved measurements appear to be insensitive to morphology. However, for all other films, the zero crossing occurs significantly earlier than 250 ps and the results are therefore not significantly affected by exciton−exciton annihilation.

When put together, the steady-state PL quenching and transient absorption data provide a complete picture of the dynamics and efficiency of exciton recombination versus charge generation in these series of films. Since the exciton diffusion length in conjugated polymers is typically between 5 and 10 nm, the observation of efficient PL quenching and ultrafast charge generation in as-spun and mildly annealed films (100 and 120 °C) is consistent with a blend morphology with phase separation on the length scale of less than 10 nm as measured by AFM. The reduction in PL quenching, decrease in charge generation efficiency, and increase in charge generation time with annealing temperature can be explained by diffusion-limited charge generation[30] coupled with the evolution of relatively pure polymer phases on the length scale of tens of nanometers. Under the assumption that the phases are relatively pure, excitons that are generated far from a domain boundary must diffuse to an interface to separate into charges. The charge generation time therefore depends on the feature size of the F8BT phases and the exciton diffusion rate. Assuming a constant exciton diffusion rate for all blends, the increasing charge generation time therefore corresponds directly to an increasing F8BT domain size with annealing. We note that for blends annealed at 180 and 200 °C the femtosecond time-resolved measurements do not show an increase in charge generation time, whereas the PL quenching is significantly reduced. This is because in the time-resolved experiments high excitation fluences are used and charges are generated by efficient exciton−exciton annihilation, which limits the observation window as discussed above.

To infer more information regarding the size and purity of the domains in these blends from the PLQE measurements, a Monte Carlo model has been developed to model the process of exciton diffusion, recombination, and dissociation. The polymer morphology was simulated by a regular 1 nm Cartesian lattice of equal amounts of F8BT- and PFB-representing sites, with the phase-separated morphology computer generated using the method of Peumans et al.,[31] which has been used successfully in device simulations.[32,33] In this method, the free energy of a random polymer network, as calculated by the Ising Hamiltonian, is minimized by a series of simulated annealing

steps. However, this method is computationally intensive when generating morphologies with domain size of greater than 20 nm. Hence an approximate technique was employed whereby a polymer morphology of extent 35 nm in each Cartesian direction and average domain size 4 nm, generated by the method of Peumans et al., was rescaled to realize morphologies with domain sizes of up to 80 nm. This approach is still likely to generate realistic morphologies as the bulk coarsening of phases is expected to proceed via spinodal decomposition that evolves through a universal, scale invariant form.[34] Even though we expect the morphologies to be realistic, it must be noted that the scaling approach artificially introduces a lower limit upon domain size (this is a problem common to the coarsest morphologies generated by the method of Peumans et al. also, which yields domains that are completely pure over length scales of tens of nanometers[33]). To preserve some minority component of each polymer within the phase of the other, domain purity was varied by swapping F8BT-representing sites with PFB-representing sites and vice-versa with probability $p_{swap}$, producing similar minority concentrations in each phase.

The processes of exciton generation, diffusion, and recombination or dissociation are simulated as follows. Excitons are injected at random F8BT-representing sites, including those representing the minority component in the PFB phase. If an exciton is adjacent to a PFB-representing site, it dissociates with unity efficiency, neglecting the possibility of unfavorable polymer orientation for the formation of charge-transfer states. Thereafter, the exciton may recombine with a probability, $p_{rec}$, which in turn determines the average exciton displacement before recombination in homogeneous material, $\lambda_d$, the exciton diffusion length. If an exciton avoids dissociation and recombination, it is then allowed to execute one step in an isotropic random walk onto a neighboring F8BT-representing site, allowing circular boundary conditions. This process is repeated until the exciton eventually dissociates or recombines. The simulation is repeated $10^6$ times to ensure reliable statistics.

Figure 5a presents exciton dissociation efficiency as predicted by the Monte Carlo simulation as a function of domain size for $0 < p_{swap} < 0.15$, for a constant exciton diffusion length of $\lambda_d = 6$ nm. Exciton dissociation efficiency decreases with increasing domain size as expected, with a strong dependence of dissociation efficiency on domain purity. Interestingly, it is seen that decreasing domain purity from 100% to 95% leads to a saturation in dissociation efficiency with increasing domain size. This is because as the domains grow the random inclusions of polymer are increasingly responsible for dissociation, making the domain boundaries and, hence, their extent less important. The observation that exciton dissociation efficiencies of more than 90% cannot be achieved for a domain purity of 95% or less places limits on the purity of the phases. If, as we assume, minority components are randomly placed, then domains must be purer than 98% to produce exciton dissociation efficiencies of less than 80%, corresponding to PLQEs of greater than 13%. We note, however, there is still likely to be some minority concentration, albeit small. If the minority components are more localized, then a lower domain purity may yield the observed PLQEs. The degree of purity in this case is hard to quantify, but the fact that PLQE drops to 13% in annealed blends suggests that the domains are highly pure over the length scale of $\lambda_d$, which itself is of the order of 10 nm. Kietzke et al. have experimentally calculated domain purities of 95% and 85% for F8BT and PFB phases, respectively, in near-thermal equilibrium phases-separated PFB:F8BT nanoparticles.[35] However, the molecular weight of F8BT used here is significantly higher and is

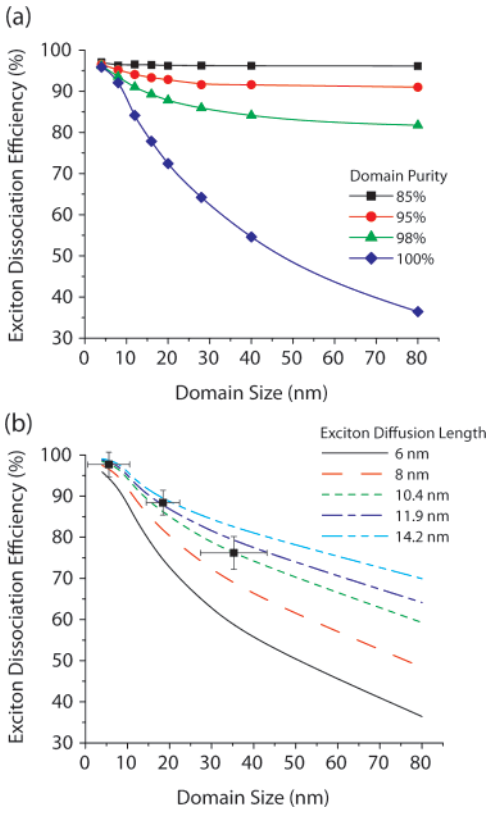


**Figure 5.** Results of Monte Carlo simulations of exciton diffusion and dissociation in simulated phase-separated blend structures with different domain sizes: (a) influence of domain purity on exciton dissociation efficiency for a fixed exciton diffusion length of 6 nm; (b) influence of exciton diffusion length on exciton dissociation efficiency modeled assuming pure domains. The data points represent exciton dissociation efficiencies calculated from PLQE measurements plotted against domain size measured by AFM.

likely to produce higher domain purities. X-ray microscopy measurements of nonequilibrium PFB:F8BT films spin-coated from xylene similarly yield a domain purity of >90% for the F8BT phase.[22] Thus, there is experimental evidence to support a relatively high domain purity. Our assumption of isotropic exciton diffusion may also influence our calculation of domain purity. Nevertheless, the observations of high PLQEs and systematically increasing charge generation times are all consistent with the prediction of our model of relatively pure phases.

Figure 5b demonstrates the influence of exciton dissociation length on exciton dissociation efficiency, with domain purity set to 100% for the purpose of this comparison. Figure 5b also plots the experimental domain size measured by AFM. Figure 5b demonstrates that exciton dissociation efficiency is further increased as the exciton diffusion length is increased. A good agreement with the experimental data is achieved for $\lambda_d = 10.4$ nm, consistent with the range of exciton diffusion lengths quoted in the literature.[9−11] This value is likely to be an overestimate given that the domains will indeed have some minority component, consistent with the recent more accurate measurements of $\lambda_d = 6$ nm.[9] Extrapolating the curve to an exciton dissociation efficiency of 51% corresponding to the 180 °C film yields an average feature size of ∼130 nm. Since this feature size is larger than the film thickness, 80 nm, surface effects will need to considered and exciton diffusion and dissociation can no longer be modeled as a bulk effect.

From consideration of charge generation efficiency alone, it would be anticipated that the as-spun film would be the most

efficient photovoltaic device as it has the highest charge generation efficiency. This is not the case; indeed device performance is optimized for a morphology with significantly reduced charge generation efficiency. This observation implies that overall device performance is determined by processes subsequent to charge generation. There are two possibilities that can account for the observed increase in device performance with decreasing charge generation efficiency. First, a more evolved phase-separated morphology may better facilitate collection of free charges through the establishment of well-defined interpenetrating networks. Thus, the efficient generation of charges in intimately mixed films cannot be exploited as there are not well-established pathways for their transport to electrodes. The other explanation is that the dissociation of excitons at a polymer−polymer interface does not directly lead to free charges but rather to bound electron−hole pairs that must be separated before they can be collected.[36] Due to the low dielectric constant of organic materials (typically $\epsilon_r = 2-3$), an electron and hole that are separated across a heterojunction following exciton dissociation still experience the Coulomb potential of the other charge. The separation of coulombically bound geminate pairs is then facilitated by a more evolved morphology that allow the charges to spatially separate more easily.[37] This explanation is supported by recent device modeling that demonstrate that impeded carrier motion during the initial separation process can indeed lead to significant geminate recombination.[32]

While directly probing the efficiency of geminate recombination is difficult, it is possible to test predictions of the charge transport-limited explanation. In particular, to explain the differences in the performance of the as-spun and annealed devices, there must be differences in the ease of charge transport through the blend. Additionally, if poor charge transport is limiting efficiency, a charge recombination mechanism must still be inferred. That is, poor charge transport can only produce a reduction in device efficiency if there are recombination channels that prevent charge from eventually being extracted. The recombination of separated charges follows a bimolecular type recombination, where charges originating from distinct photoexcitations recombine. As the probability of recombination increases with increasing charge density, bimolecular recombination appears as a nonlinear dependence of photocurrent on light intensity. For the case of geminate recombination, where electrons and holes recombine with their geminate partner, recombination follows a monomolecular process and would be accompanied by a linear dependence of photocurrent on intensity.

First, to investigate charge transport, the current−voltage characteristics of hole-only devices have been measured, Figure 6a. These curves have been fitted to the space-charge-limited expression

$$J_{SCL} = \frac{9}{8}\epsilon\mu_0 \exp[0.891\gamma\sqrt{V_{int}/L}]\frac{V_{int}^{\ 2}}{L^3} \qquad (1)$$

that accounts for a field-dependent mobility of the form $\mu = \mu_0 \exp(\gamma\sqrt{E})$, where $\mu_0$ is the zero-field mobility, $\gamma$ the field activation parameter, $E$ the electric field strength, $J_{SCL}$ the current density, $\epsilon$ the permittivity, $V_{int}$ the internal voltage, and $L$ the film thickness. The fitted mobilities are displayed in Figure 6a, using a relative permittivity $\epsilon_r = 3$ and $\gamma$ of 0.5 to 4 × $10^{-4}$ $(m/V)^{0.5}$. (See Supporting Information for further details.) Compared to a pristine PFB film mobility of 1.5 × $10^{-7}$ $cm^2/Vs$, the mobilities of the 100−140 °C annealed films are only slightly lower, at ∼1 × $10^{-7}$ $cm^2/Vs$. This result is somewhat surprising as it demonstrates that the additional disorder of a blended film does not significantly affect charge transport. This may reflect the fact that films of amorphous conjugated polymers are already highly disordered with charges following highly convoluted pathways such that accommodating the presence of another polymer in a blend makes no significant difference to overall mobility. Also, these results suggest that in the case of all-polymer blends sufficiently interconnected networks are already present even in intimately mixed blends. Significantly, however, these results show that there is little difference in mobility for 100, 120, and 140 °C annealed films that would explain the increase in device efficiency with annealing to 140 °C in terms of improved charge transport. While there is a significant improvement in mobility with the 160 °C annealed film, device performance has already begun to deteriorate, further implying that charge transport is not limiting efficiency.

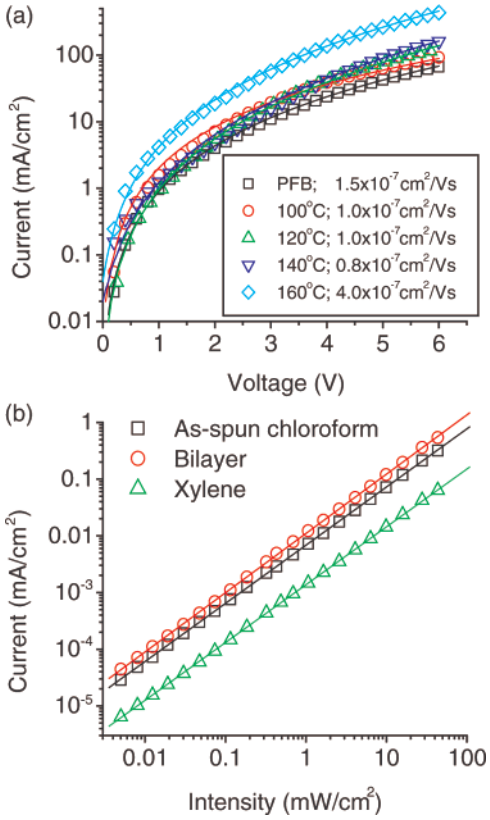


**Figure 6.** (a) Current−voltage curves of hole-only devices with fits to the space-charge-limited model. (b) Intensity dependence of short-circuit current for as-spun chloroform, xylene, and bilayer PFB:F8BT devices.

Investigating now the intensity dependence of short-circuit current ($J_{SC}$), Figure 6b compares the intensity dependence of an as-spun chloroform device, a xylene-processed device[13] (1:1 weight ratio), and a PFB/F8BT bilayer device (prepared by first spin-coating a pristine PFB film and then laminating an F8BT layer on top with a total thickness of 80 nm). Note that since monochromatic light with a wavelength that matches the absorption maximum of F8BT was used (470 nm), the maximum intensity of ∼50 $mW/cm^2$ employed here actually corresponds to an equivalent intensity of 500 $mW/cm^2$ AM1.5G irradiation. Figure 6b shows that, despite the vastly different morphologies of the three devices, all devices exhibit a linear dependence of $J_{SC}$ on light intensity over 4 orders of magnitude ($\alpha = 1.0$ for all devices where $J_{SC} \propto I^{\alpha}$ and $I$ is the incident light intensity).

Given that the intensity dependence of an intimately mixed blend is the same as a bilayer with large, pure phases implies that recombination due to poor charge transport is not significant and cannot explain the differences in efficiency observed.

We conclude, therefore, that geminate recombination and not charge transport is responsible for the low efficiency of intimately mixed PFB:F8BT films. Furthermore, we can account for the low efficiency of PFB:F8BT blends in general in terms of this strong geminate recombination. By controlling the morphology on a length scale of tens of nanometers, we have demonstrated that geminate recombination is so severe that to optimize device performance requires morphology to evolve to such extent that exciton dissociation efficiency drops significantly. The difficulty separating geminate electron−hole pairs in blends with a spatially confined geometry easily explains why bilayer devices with only one planar interface for charge generation are more efficient than as-spun chloroform blends (Figure 5). Accounting for poor device performance in terms of geminate recombination also provides a self-consistent explanation for the low performance of PFB:F8BT blends that is observed regardless of morphology,[12,13] device geometry, or blend ratio.[13,22] The origin of the fast geminate recombination rate appears to be particular to this combination of polymers, as much higher efficiencies have been demonstrated for other all-polymer devices.[6,38,39] Indeed, a power conversion efficiency of 1.8% has been recently demonstrated using a red polyfluorene that has 1 order of magnitude lower electron mobility that that for F8BT.[6] Therefore, an explanation of poor charge transport to account for the performance of PFB:F8BT blends appears to be at odds with the observation that higher efficiencies can be achieved with polymers with lower charge carrier mobilities. The origin of the strong geminate recombination in PFB:F8BT blends is likely to be due to the nature of interfacial interactions between neighboring PFB and F8BT chains. Recent work by Sreearunothai et al.[40] has shown that different chain orientations of PFB and F8BT at a heterojunction interface can lead to either a repulsive barrier or attractive interaction that can either enhance or suppress charge separation. Additionally, the efficiency of blends of PCBM with various polyfluorene copolymers has been correlated with the degree of ground-state charge transfer that exists between the materials.[41] Therefore the nature of interfacial interactions appears to be a stronger determinant of the photovoltaic efficiency of a particular polymer−polymer combination than variations in charge transport. (Interestingly, possible changes in interfacial interactions with annealing may also play a role in the trends observed here, and further work would be required to separate these effects. However microscopic modeling predicts an increase in charge separation due purely to an increase in domain size without a change in interfacial interactions.[32]) Future device improvements should therefore consider tuning of intermolecular interactions to enhance charge separation and suppress geminate recombination.

The results presented here also have implications for the design of ideal polymer blend morphologies. We have shown that for PFB:F8BT blends the optimum length of phase separation is of order 20 nm, significantly larger than the exciton diffusion length of 5−10 nm[9] but comparable to the thermal capture radius of 15−20 nm. This observation demonstrates that the efficiency of geminate pair separation is just an important parameter in determining optimum domain size as exciton diffusion length. In other words, when one is designing an ideal morphology, the length scale of phase separation must be selected to balance charge generation with charge separation. For the system studied here, due to the high efficiency of geminate recombination, engineering of an ideal, interdigitated morphology with spacing of 20 nm would not necessarily produce devices with higher external quantum efficiencies than efficient all-polymer blend[6] or polymer/fullerene[3] devices with higher charge separation efficiencies. While highly ordered, well-defined morphologies will undoubtedly enhance device performance, attention must also be placed on suppressing geminate recombination.

## Conclusions

Through controlled annealing of intimately mixed PFB:F8BT blends, we have observed the influence of nanoscale phase separation on charge generation and device performance as the length scale of phase separation evolves from less than 10 nm to more than 40 nm. We find that device efficiency is optimized for a phase separation of ∼20 nm, significantly larger than the exciton diffusion length. Femtosecond transient absorption confirms that charge generation is more efficient in more intimately mixed blends, with the charge generation time increasing systematically as blend morphology evolves. Photoluminescence measurements also confirm that charge generation efficiency decreases with evolving phase separation. These PL and transient absorption measurements suggest that charge generation is diffusion-limited, with exciton dissociation occurring largely at domain interfaces. From Monte Carlo modeling of exciton diffusion and dissociation we find consistency between the PLQE of annealed films and their measured domain sizes and infer that these nanoscale domains must be >95% pure. Studying charge transport through PFB:F8BT blends and the intensity dependence of photocurrent, we have shown that charge transport does not significantly improve as device performance improves and that there is no evidence of bimolecular recombination that should accompany a charge transport-limited mechanism. We conclude therefore that device performance is limited by geminate recombination and not charge transport, with the observed optimal phase separation of 20 nm balancing the efficiencies of charge generation and charge separation.

**Acknowledgment.** This work was supported by the Engineering and Physical Sciences Research Council of the U.K. (SUPERGEN IV). We thank Cambridge Display Technology Ltd. for the supply of conjugated polymers used in this study. S.W. thanks Fitzwilliam College, Cambridge, U.K., for a Junior Research Fellowship.

**Supporting Information Available:** Ultraviolet to visible absorption spectra of blend films as a function of annealing temperature, dependence of fill factor and open circuit voltage on annealing temperature, and further details of space-charge-limited current−voltage fits. This material is available free of charge via the Internet at http://pubs.acs.org.

## References and Notes

(1) Gunes, S.; Neugebauer, H.; Sariciftci, N. S. *Chem. Rev.* **2007**, *107*, 1324−1338.
(2) Kim, J. Y.; Lee, K.; Coates, N. E.; Moses, D.; Nguyen, T. Q.; Dante, M.; Heeger, A. J. *Science* **2007**, *317*, 222−225.
(3) Peet, J.; Kim, J. Y.; Coates, N. E.; Ma, W. L.; Moses, D.; Heeger, A. J.; Bazan, G. C. *Nat. Mater.* **2007**, *6*, 497−500.
(4) Halls, J. J. M.; Walsh, C. A.; Greenham, N. C.; Marseglia, E. A.; Friend, R. H.; Moratti, S. C.; Holmes, A. B. *Nature* **1995**, *376*, 498−500.
(5) Yu, G.; Gao, J.; Hummelen, J. C.; Wudl, F.; Heeger, A. J. *Science* **1995**, *270*, 1789−1791.
(6) McNeill, C. R.; Abrusci, A.; Zaumseil, J.; Wilson, R.; McKiernan, M. J.; Halls, J. J. M.; Greenham, N. C.; Friend, R. H. *Appl. Phys. Lett.* **2007**, *90*, 193506.

(7) Jenekhe, S. A.; Chen, X. L. *Science* **1999**, *15* (283), 372−375.
(8) Lindner, S. M.; Huttner, S.; Chiche, A.; Thelakkat, M.; Krausch, G. *Angew. Chem., Int. Ed.* **2006**, *45* (20), 3364−3368.
(9) Markov, D. E.; Amsterdam, E.; Blom, P. W. M.; Sieval, A. B.; Hummelen, J. C. *J. Phys. Chem. A* **2005**, *109* (24), 5266−5274.
(10) Halls, J. J. M.; Pichler, K.; Friend, R. H.; Moratti, S. C.; Holmes, A. B. *Appl. Phys. Lett.* **1996**, *68*, 3120.
(11) Haugeneder, A.; Neges, M.; Kallinger, C.; Spirkl, W.; Lemmer, U.; Feldmann, J.; Scherf, U.; Harth, E.; Gugel, A.; Müllen, K. *Phys. Rev. B* **1999**, *59* (23), 15346−15351.
(12) Halls, J. J. M.; Arias, A. C.; MacKenzie, J. D.; Wu, W.; Inbasekaran, M.; Woo, E. P.; Friend, R. H. *Adv. Mater.* **2000**, *12*, 498−502.
(13) Snaith, H. J.; Arias, A. C.; Morteani, A. C.; Silva, C.; Friend, R. H. *Nano Lett.* **2002**, *2* (12), 1353−1357.
(14) Snaith, H. J.; Greenham, N. C.; Friend, R. H. *Adv. Mater.* **2004**, *16*, 1640−1645.
(15) Ramsdale, C. M.; Barker, J. A.; Arias, A. C.; MacKenzie, J. D.; Friend, R. H.; Greenham, N. C. *J. Appl. Phys.* **2002**, *92* (8), 4266−4270.
(16) Morteani, A. C.; Dhoot, A. S.; Kim, J. S.; Silva, C.; Greenham, N. C.; Murphy, C.; Moons, E.; Ciná, S.; Burroughes, J. H.; Friend, R. H. *Adv. Mater.* **2003**, *15*, 1708−1712.
(17) Morteani, A. C.; Sreearunothai, P.; Herz, L. M.; Friend, R. H.; Silva, C. *Phys. Rev. Lett.* **2004**, *92* (24), 7402.
(18) Arias, A. C.; MacKenzie, J. D.; Stevenson, R.; Halls, J. J. M.; Inbasekaran, M.; Woo, E. P.; Richards, D.; Friend, R. H. *Macromolecules* **2001**, *34*, 6005−6013.
(19) McNeill, C. R.; Frohne, H.; Holdsworth, J. L.; Dastoor, P. C. *Nano Lett.* **2004**, *4* (12), 2503−2507.
(20) Coffey, D. C.; Ginger, D. S. *Nat. Mater.* **2006**, *5*, 735−740.
(21) McNeill, C. R.; Watts, B.; Thomsen, L.; Belcher, W. J.; Greenham, N. C.; Dastoor, P. C. *Nano Lett.* **2006**, *6* (6), 1202−1206.
(22) McNeill, C. R.; Watts, B.; Thomsen, L.; Ade, H.; Greenham, N. C.; Dastoor, P. C. *Macromolecules* **2007**, *40* (9), 3263−3270.
(23) de Mello, J. C.; Wittmann, H. F.; Friend, R. H. *Adv. Mater.* **1997**, *9*, 230−232.
(24) Manzoni, C.; Polli, D.; Cerullo, G. *Rev. Sci. Instrum.* **2006**, *77*, 023103.
(25) Donley, C. L.; Zaumseil, J.; Andreasen, J. W.; Nielsen, M. M.; Sirringhaus, H.; Friend, R. H.; Kim, J. S. *J. Am. Chem. Soc.* **2005**, *127*, 12890−12899.
(26) Bernius, M.; Inbasekaran, M.; Woo, E.; Wu, W.; Wujkowski, L. *J. Mater. Sci.: Mater. Electron.* **2000**, *11*, 111−116.
(27) Yin, C.; Kietzke, T.; Neher, D.; Hörhold, H. H. *Appl. Phys. Lett.* **2007**, *90*, 092117.
(28) Stevens, M. A.; Silva, C.; Russell, D. M.; Friend, R. H. *Phys. Rev. B* **2001**, *63*, 165213.
(29) Takeda, S.; Asaoka, S.; Miller, J. R. *J. Am. Chem. Soc.* **2006**, *128*, 16073−16082.
(30) Westenhoff, S.; Hayes, S. C.; Greenham, N. C.; Silva, C. In *Charge Generation in Inorganic/Organic Photovoltaic Blends*; Proceedings of the 14th International Conference on Ultrafast Phenomena, Niigata, Japan, 2004; Kobayashi, T., Okada, T., Kobayashi, T., Nelson, K. A., De Silvestri, S., Eds.; Springer: Niigata, Japan, 2004; pp 783−785.
(31) Peumans, P.; Uchida, S.; Forrest, S. R. *Nature* **2003**, *425*, 158−162.
(32) Marsh, R. A.; Groves, C.; Greenham, N. C. *J. Appl. Phys.* **2007**, *101*, 083509.
(33) Watkins, P. K.; Walker, A. B.; Verschoor, G. L. B. *Nano Lett.* **2005**, *5*, 1814−1818.
(34) Bates, F. S. *Science* **1991**, *251*, 898−905.
(35) Kietzke, T.; Neher, D.; Kumke, M.; Ghazy, O.; Ziener, U.; Landfester, K. *Small* **2007**, *3* (6), 1041−1048.
(36) Mihailetchi, V. D.; Koster, L. J. A.; Hummelen, J. C.; Blom, P. W. M. *Phys. Rev. Lett.* **2004**, *93* (21), 216601.
(37) Quist, P. A. C.; Savenije, T. J.; Koetse, M. M.; Veenstra, S. C.; Kroon, J. M.; Siebbeles, L. D. A. *Adv. Funct. Mater.* **2005**, *15*, 469−474.
(38) Koetse, M. M.; Sweelssen, J.; Hoekerd, K. T.; Schoo, H. F. M.; Veenstra, S. C.; Kroon, J. M.; Yang, X.; Loos, J. *Appl. Phys. Lett.* **2006**, *88*, 083504.
(39) Kietzke, T.; Hörhold, H.-H.; Neher, D. *Chem. Mater.* **2005**, *17*, 6532−6537.
(40) Sreearunothai, P.; Morteani, A. C.; Avilov, I.; Cornil, C.; Beljonne, D.; Friend, R. H.; Phillips, R. T.; Silva, C.; Herz, L. M. *Phys. Rev. Lett.* **2006**, *96*, 117403.
(41) Benson-Smith, J. J.; Goris, L.; Vandewal, K.; Haenen, K.; Manca, J. V.; Vanderzande, D.; Bradley, D. C.; Nelson, J. *Adv. Funct. Mater.* **2007**, *17*, 451−457.